Journal of Molecular Liquids 232 (2017) 423–430

Contents lists available at ScienceDirect

Journal of Molecular Liquids

journal homepage: www.elsevier.com/locate/molliq

Degradation of azo dyes under different wavelengths of UV light with chitosan-SnO2 nanocomposites

Vinod Kumar Gupta [a,*], R. Saravanan [b,*], Shilpi Agarwal [a], F. Gracia [b], Mohhammad Mansoob Khan [c], Jiaqian Qin [d], R.V. Mangalaraja [e]

[a] Department of Applied Chemistry, University of Johannesburg, Johannesburg, South Africa
[b] Department of Chemical Engineering and Biotechnology, University of Chile, Beauchef 850, Santiago, Chile
[c] Chemical Sciences, Faculty of Science, Universiti Brunei Darussalam, Jalan Tungku, Link, BE1410, Brunei Darussalam
[d] Metallurgy and Materials Science Research Institute, Chulalongkorn University, Bangkok 10330, Thailand
[e] Advanced Ceramics and Nanotechnology Laboratory, Department of Materials Engineering, University of Concepcion, Concepcion, Chile

ARTICLE INFO

Article history:
Received 31 January 2017
Received in revised form 21 February 2017
Accepted 22 February 2017
Available online 27 February 2017

Keywords:
Chitosan-SnO_2
Nanocomposites
UV light
Photocatalyst

ABSTRACT

In this study, synthesis of novel binary chitosan-SnO_2 nanocomposites is reported. Different physical and chemical techniques were used to characterize and analyze the characteristics of the chitosan-SnO_2 nanocomposites as photocatalysts. The prepared novel photocatalysts were used to degrade the model dyes such as methyl orange (MO) and rhodamine B (RhB) under different wavelengths (254, 310 and 365 nm) of UV light. The photocatalytic degradation results suggest that the prepared binary chitosan-SnO_2 (50:50) nanocomposite shows superior degradation efficiency compared with pure SnO_2 and binary chitosan-SnO_2 (75:25) nanocomposite owing to its high crystallinity, high surface area, and small particle size. It was also observed that chitosan-SnO_2 (50:50) nanocomposite under different wavelengths (254 nm, 310 nm, and 365 nm) of UV light showed highest photocatalytic degradation of methyl orange and rhodamine B at 365 nm irradiation.

1. Introduction

In the recent years, researchers have started focusing on the removal of toxic organic pollutants present in the wastewater due to creating major health and environmental problems. It is an immense need of human beings to recycle wastewater because usage of water is becoming almost doubled at every two decades [1]. The United Nations has reported that every day about 2 million tons of sewage, agricultural and industrial wastes are discharged into the world's natural water resources [2]. It has also estimated that about 1500 km^3 amount of wastewater produced annually, that is about six times more water than that exists in all the rivers across the world [2,3]. Therefore, removal of organic pollutants from the waste water is significant and a major environmental concern all over the world. Though several methods and technologies have been developed for the treatment of waste water but heterogeneous photocatalytic treatment is one of the green ways to purify the waste water. This process has several advantages like simple processing, no or very less secondary pollutants, no waste disposal, no need of any special equipment and a promising cost-effective way [1,4].

Nowadays, semiconductors such as nano-sized metal oxides have attained more importance in the field of photocatalysis due to their excellent efficiency of degrading various pollutants [5]. Over the past few decades, semiconductor metal oxides such as zinc oxide (ZnO) and titanium dioxide (TiO_2) are considered to be the most studied and efficient photocatalysts because of their uses as photocatalysts are cost effective, poses a low risk to the environment and exhibits high stability [6–8]. Apart from these, tin oxide (SnO_2) is one of the large band gap semiconducting materials having lots of advantages and broad applications in electronic and optoelectronic devices, solar cells, gas sensors and heterogeneous catalysis [9,10].

The photocatalytic degradation rate of SnO_2 can be further enhanced by various methods such as combining or coupling SnO_2 with metal or metal oxides, doping with different metal ions into SnO_2 and making polymer composites [10–13]. Chitosan (CS) is found to be the most abundant natural biopolymer having great fascinating properties such as inexpensive, non-toxic, bio and eco-friendly. CS contains two functional groups such as hydroxyl and amino groups. These groups impart various properties to synthesize materials such as antimicrobial activity, gas sensing, and wastewater treatment ability [14–16]. Recently, Xiao et al. have reported that CS-TiO_2 nanocomposite has effectively degraded methyl orange [14]. Dehaghi et al. have also reported that due to

* Corresponding authors.
E-mail addresses: vinodg@uj.ac.za (V.K. Gupta), saravanan3.raj@gmail.com (R. Saravanan).

http://dx.doi.org/10.1016/j.molliq.2017.02.095
0167-7322/

adsorbing property of CS, the CS-ZnO nanobeads efficiently remove the permethrin pesticide from water [17].

In the present work, pure SnO_2 and binary CS-SnO_2 nanocomposites were synthesized by precipitation method followed by sonication. To the best of our knowledge, this is the first report of CS-SnO_2 nanocomposite used for photocatalytic degradation of organic dyes under different wavelengths of UV light. The structure, shape, size, and optical band gap of the prepared photocatalysts were characterized and confirmed by X-ray diffraction (XRD), transmission electron microscopy (TEM), and diffuse reflectance spectroscopy (DRS), respectively. Finally, the prepared photocatalysts were used to degrade methyl orange (MO) and rhodamine B (RhB) aqueous solutions separately under different wavelengths of UV light (365, 310 and 254 nm).

2. Experimental

2.1. Methods

The powder X-ray diffraction technique was used to find the crystal structure and crystallite size of the synthesized materials at room temperature using a D5000 diffractometer (Siemens, USA) with $CuK_{\alpha 1}$ ($\lambda = 1.5406$ Å) radiation. The shape and size of the synthesized materials were confirmed by transmission electron microscopy (TEM, Tecnai G^2 20 S-TWIN, FEI Netherlands). The specific surface area of the catalysts was calculated using Brunauer–Emmett–Teller (BET, Micromeritics ASAP 2020, USA). The optical band gap of the prepared materials was determined from the UV–Vis diffuse reflectance spectra which were recorded at room temperature using UV-VIS-NIR Spectrophotometer (VARIAN CARY 5E, USA). The photocatalytic activity was measured by using a UV–Visible spectrophotometer (Perkin Elmer Lambda 35, USA).

2.2. Materials

For the synthesis of pure SnO_2 and CS-SnO_2 nanocomposites, the required chemicals such as tin (II) acetate, chitosan, ammonia, acetic acid and citric acid, and for the photocatalytic degradation, the dyes such as methyl orange (MO) and rhodamine B (RhB), were procured from Sigma-Aldrich. These chemicals were used without any further purification. All the aqueous solutions were prepared using double distilled water.

2.3. Preparation of pure SnO_2 nanoparticles

The pure SnO_2 nanoparticles were prepared by precipitation method which is one of the simple and cost-effective routes for the preparation of the nanomaterials. At first, 5.0 g of tin (II) acetate was refluxed in 300 mL of ammonia in a 500 mL round bottom flask for 24 h. Then, 0.05 mol of aqueous citrate solution was added dropwise into the refluxed solution under stirring at 0 °C for 2 h, and finally, a white gel was formed. The gel was allowed drying for 10 days at room temperature and a white dry powder was obtained. It was transferred to the mortar for grinding. The finely grounded powder sample was later transferred into an alumina boat and calcinated at 350 °C for 30 min.

2.4. Preparation of CS-SnO_2 nanocomposites

For the preparation of nanocomposite, 1.0 g of chitosan was mixed with 0.5 g (50 wt%) of the prepared SnO_2 nanoparticles and the mixed powder was dissolved in 100 mL of 1% (v/v) acetic acid in a 250 mL beaker. The pH of the solution was maintained between 7 and 8 by using ammonia. The dissolved solution was sonicated (~40 kHz) overnight and finally, the CS-SnO_2 nanocomposite was separated by centrifuge at 15000 rpm. The sample was recovered and followed by filtering, washing, and finally drying at 50 °C for 10 h. The nanocomposite was labeled as CS-SnO_2 (50:50). Similarly, CS-SnO_2 (75:25) nanocomposite was prepared by taking 2.0 g of chitosan with 0.5 g (25 wt%) of SnO_2 by the above-mentioned procedure.

2.5. Photocatalytic activity

The photocatalytic procedure was followed as reported in the previous literature [8]. The synthesized materials were used as photocatalysts for the degradation of aqueous methyl orange (MO) and rhodamine B (RhB) dye solutions separately under different wavelengths, i.e. 365, 310 and 254 nm of UV light irradiation. The concentration of dyes was 5×10^{-5} mol/L. The source of UV light (8 W mercury vapor lamp with different wavelengths 365, 310 and 254 nm) was sealed in cylindrical quartz glass tube to prevent direct contact with the dye solution. At first, the photolysis of the aqueous MO and RhB dye solutions were tested without a catalyst under the dark condition for 100 min under UV light irradiation. The concentrations of the irradiated samples were observed using UV–Visible spectrophotometer and it was found that there was no decoloration. This shows that UV light alone cannot degrade the dyes. These results confirm that the dyes were quite stable under UV light irradiation.

The photocatalytic suspension was prepared by taking 100 mg of synthesized photocatalysts in 100 mL of aqueous dye solution in a 250 mL cylindrical beaker containing water jacket so as to maintain a constant temperature (25 °C). The suspension was magnetically stirred under a dark condition for 20 min to establish adsorption/desorption equilibrium condition. The suspensions were irradiated with the different wavelength of UV light. The irradiated sample was collected at every 20 min and the sample was centrifuged, filtered and the concentrations of the irradiated dye solutions were monitored using a UV–Visible spectrophotometer. The degradation efficiencies of MO and RhB were calculated using the following formula:

$$\eta = \left[1 - \frac{C}{C_0}\right] \times 100 \quad (1)$$

where, η is the degradation efficiency, C_0 and C are the concentrations of the dye solution before illumination ($t = 0$) and after illumination of light for 't' minutes, respectively.

3. Results and discussion

In this study, synthesis of pure SnO_2 nanoparticles and binary chitosan-SnO_2 nanocomposites were based on the precipitation method followed by sonication. This method is simple and cost effective compared with other methods. In the present study, it has been shown

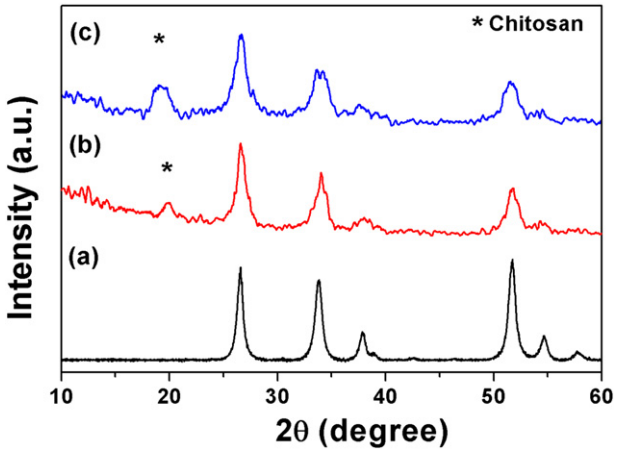

Fig. 1. XRD patterns of (a) pure SnO_2, (b) CS-SnO_2 (50:50), and (c) CS-SnO_2 (75:25).

Table 1
Crystallite size, BET surface area, TEM particle size and band gap of the synthesized binary CS-SnO_2 photocatalysts.

Samples	Crystallite size D (nm)	BET surface area (m^2/g)	TEM Particle size (nm)	Reflectance edge (nm)	Band gap based on KM function (eV)
Pure SnO_2	13.2	73.2	15	364	3.38
CS-SnO_2 (50:50)	8.4	84.1	11	348	3.52
CS-SnO_2 (75:25)	6.7	89.2	Agglomeration	318	3.91

that the binary chitosan-SnO_2 nanocomposites were used as photocatalysts for the degradation of model dyes such as methyl orange and rhodamine B under different wavelengths (i.e. 365, 310 and 254 nm) of UV light irradiation and the photocatalysts were effectively degraded the dyes.

The structure and crystallite size of the prepared photocatalysts were investigated using XRD analysis. The XRD pattern of pure SnO_2 nanoparticles is shown in Fig. 1(a). It clearly shows that there are several sharp diffraction peaks, which confirms that the synthesized material is pure and crystalline in nature. The diffraction peaks are indexed and the 2θ values are obtained at 26.5°, 33.8°, 37.8°, 38.9°, 51.7°, 54.7° and 57.8° and their corresponding h k l planes were identified as (110), (101), (200), (111), (211), (220) and (002), respectively. These values are in agreement with the tetragonal structure of SnO_2 nanoparticles (JCPDS No: 88-0287). Furthermore, no any other impurities were found in the samples.

The XRD patterns of CS-SnO_2 (50:50) and CS-SnO_2 (75:25) are represented in Fig. 1(b) and (c), respectively. The XRD patterns showed that after introducing chitosan into SnO_2 no any change in the tetragonal structure of SnO_2 was observed. In case of nanocomposites, the chitosan peaks were observed at 19.9° highlighted by (*) in Fig. 1(b) and (c). Compared with pure SnO_2 pattern, the CS-SnO_2 nanocomposites patterns showed broader and lower intensity peaks. If the peaks are broader the materials may have small crystallite size and low intensity peaks are due to the decrease in the crystallinity of the nanomaterials [8]. This is due to the intermolecular interaction and synergistic effect between chitosan and SnO_2 in the nanocomposites [18,19].

The crystallite size (D) of the prepared photocatalysts was calculated using Scherrer formula:

$$D = k\lambda/\beta\cos\theta \quad (2)$$

where k is the shape factor (0.89), λ is the wavelength of X-ray (1.5406 Å), β is the line broadening at full width at half maximum (FWHM) in radians, and θ is the Bragg's angle. Table 1 illustrates the values of the crystallite size of the synthesized photocatalysts. The broadened diffraction peaks of the nanocomposites are indicative of their smaller size, whereas the narrow and sharp peaks of pure SnO_2 is due to larger crystallite size. Small size leads to high surface area which was confirmed by BET analysis and the results of BET specific surface areas are also tabulated in Table 1. The specific surface area of CS-SnO_2 nanocomposites has increased because of the synergistic effect between chitosan and SnO_2 nanoparticles which leads to small size of nanocomposites [11,20].

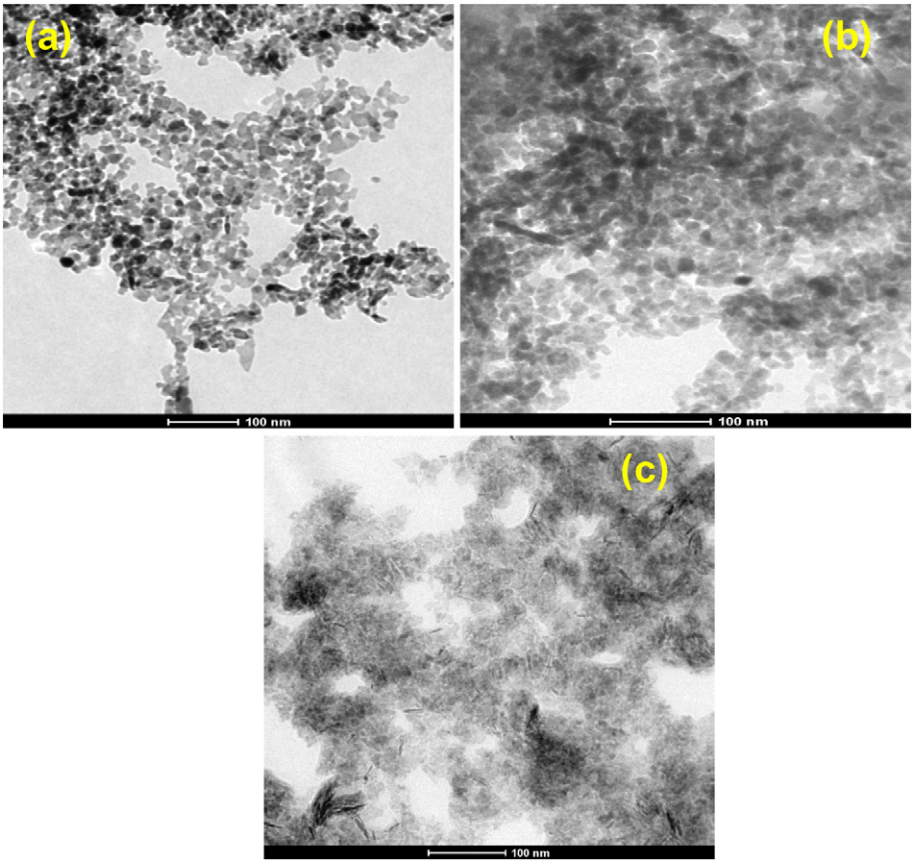

Fig. 2. TEM images of (a) pure SnO_2, (b) CS-SnO_2 (50:50) and (c) CS-SnO_2 (75:25).

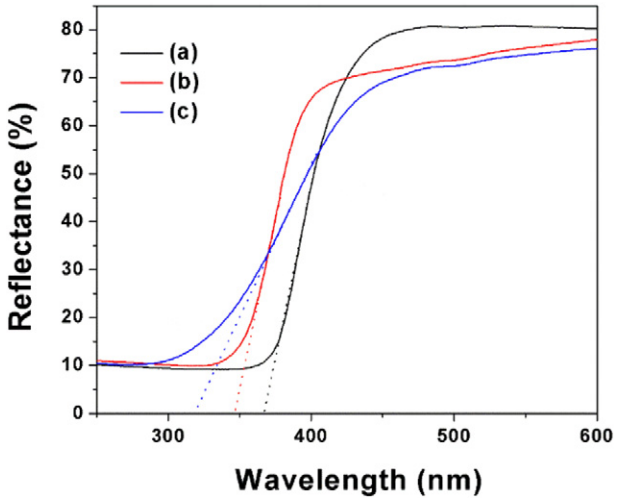

Fig. 3. DRS spectra of (a) pure SnO_2, (b) CS-SnO_2 (50:50) and (c) CS-SnO_2 (75:25).

TEM images are used to study the shape and size of the prepared photocatalysts. In Fig. 2(a), the TEM image of pure SnO_2 nanoparticle visibly revealed the presence of quite a big number of fine spherical shaped nanoparticles. The TEM images of CS-SnO_2 (50:50) and CS-SnO_2 (75:25) nanocomposites are illustrated in Fig. 2(b) and (c) respectively. Fig. 2(b) shows the CS-SnO_2 (50:50) nanocomposite which clearly specifies that the SnO_2 nanoparticles are embedded in the chitosan matrix. After increasing the chitosan quantity into SnO_2, the TEM image for CS-SnO_2 (75:25) is shown in Fig. 2(c) which clearly shows that the SnO_2 nanoparticles are dispersed and give more aggregation due to the intermolecular interaction between chitosan and SnO_2 nanoparticles [21]. A similar observation is reported in the literature [21]. The particle sizes were determined and the values are presented in Table 1.

The optical band gap of all the synthesized photocatalysts were determined using DRS spectra and their corresponding plots are shown in Fig. 3. From the figure it appears that the reflectance edge of the nanocomposites are at lower wavelength than that of pure SnO_2 nanoparticles. The reflectance edges around 364, 348 and 318 nm correspond to the SnO_2, CS-SnO_2 (50:50) and CS-SnO_2 (75:25), respectively.

The band gap value of the prepared sample was determined from the Kubelka – Munk (KM) relation:

$$F(R) = \frac{(1-R)^2}{2R} \quad (2)$$

where R is the reflectance of the sample.

Based on the equation, $(F(R) * E)^{1/2}$ vs. photon energy (E). the band gap values were calculated and the values are tabulated in Table 1. The band gap of CS-SnO_2 (75:25) is higher when compared with other prepared photocatalysts, because of the quantum confinement of charge carriers i.e. decrease in the size of CS-SnO_2 (75:25) nanocomposite [8]. Thus, when compared with the other two synthesized samples, the size of CS-SnO_2 (75:25) nanocomposite is small and this result is in an agreement with TEM and XRD analyses. From the DRS spectra, it is clear that all the prepared photocatalysts showing absorption in the UV region of the electromagnetic spectrum. Therefore, we concluded that because of strong absorption in the UV region, it is expected that the synthesized photocatalysts could be photocatalytically active under UV light irradiation.

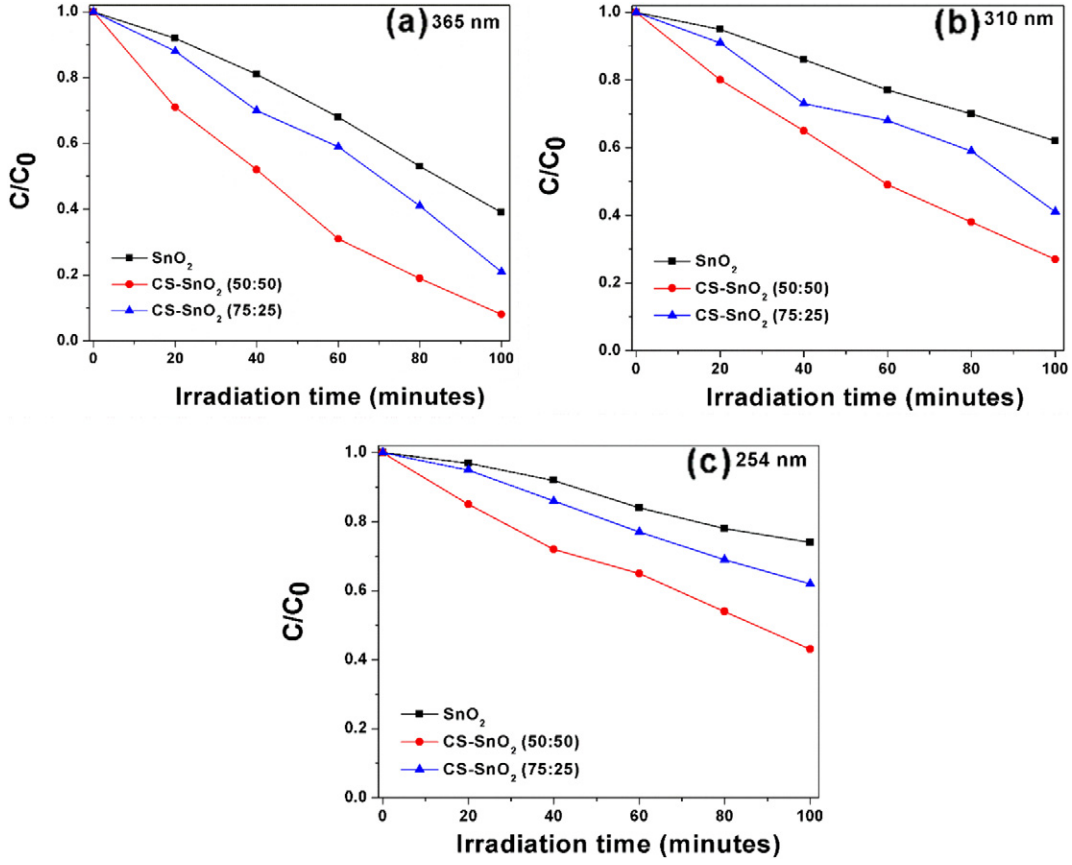

Fig. 4. Time course degradation curves for MO using prepared photocatalysts under different wavelengths (a) 365 nm, (b) 310 nm, and (c) 254 nm of UV light.

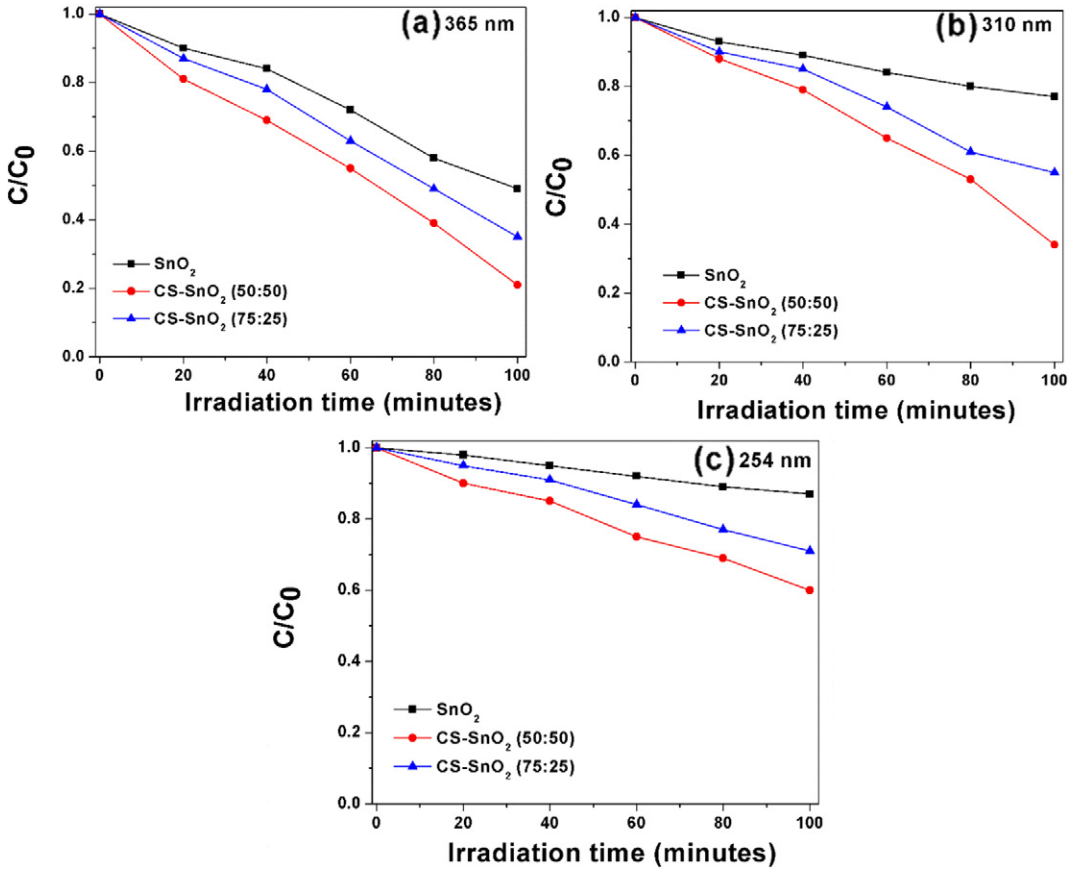

Fig. 5. Time course degradation curves for RhB using prepared photocatalysts under different wavelengths (a) 365 nm, (b) 310 nm, and (c) 254 nm of UV light.

3.1. Photocatalytic degradation of dyes

The photocatalytic degradation process involves degradation of model dyes such as MO and RhB using the synthesized binary photocatalysts under different wavelengths (i.e. 365, 310 and 254 nm) of UV light irradiation. Their consistent time course degradation curves are represented in the Figs. 4 and 5, respectively.

From the figure it is clear that the degradation efficiency increases with increasing irradiation time. When compared with pure SnO_2 degradation results, the nanocomposites are found to have higher degradation efficiency. This is because chitosan has amino and hydroxyl groups that enhances the performance of the photocatalytic activities of the synthesized nanocomposites by providing reactive sites for dyes [17,18].

The degradation efficiency of prepared photocatalysts was calculated using Eq. (1) and the values are listed in Table 2. Compared with RhB degradation, MO has degraded at much faster than the RhB because MO is anionic dye which facilitates the enhancement of photocatalytic reaction, whereas RhB is a cationic dye. During the photocatalytic reaction, the repulsive forces between RhB and the nanocomposites may reduce its degradation efficiency [14]. Therefore, the degradation rate for RhB is lower when compared with that of MO degradation rate. From the obtained results, it was observed that degradation efficiency increases with wavelength of UV light, that is 365 nm > 310 nm > 254 nm. This is because of the inability of shorter wavelength to excite more electrons during the photocatalytic reactions [22].

The first order rate constants (k) of the photocatalytic reactions were calculated from the following equation:

$$k = \ln(C/C_0)/t \quad (3)$$

Table 2
Degradation efficiency and rate constants of the prepared binary photocatalysts.

Samples	Wavelength of UV light (nm)	Degradation efficiency (MO) duration 100 min	First order rate constant k (MO) 10^{-4} min^{-1}	Degradation efficiency (RhB) duration 100 min	First order rate constant k (RhB) 10^{-4} min^{-1}
SnO_2	365	61%	0.810	51%	0.653
	310	38%	0.410	24%	0.275
	254	26%	0.290	13%	0.138
CS-SnO_2 (50:50)	365	92%	2.220	79%	1.301
	310	73%	1.240	66%	0.889
	254	57%	0.800	41%	0.484
CS-SnO_2 (75:25)	365	79%	1.250	65%	0.920
	310	59%	0.768	43%	0.571
	254	39%	0.450	29%	0.319

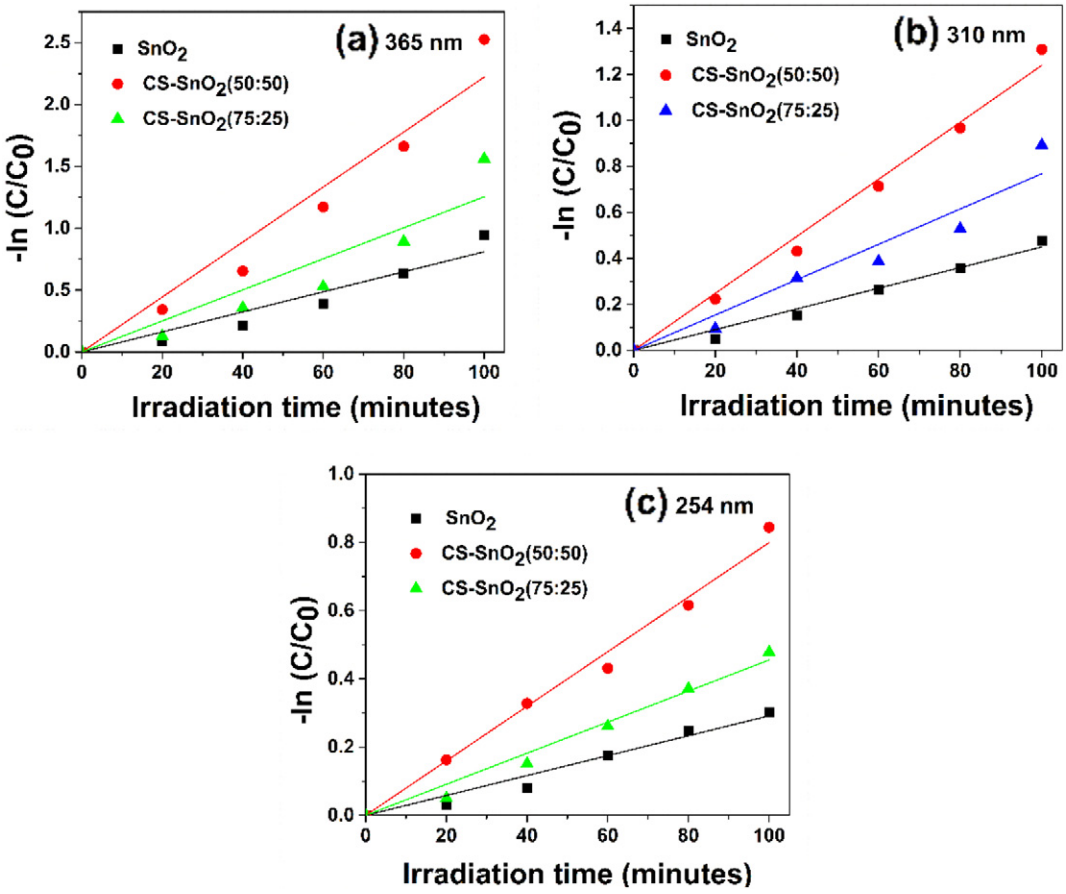

Fig. 6. Plots of $\ln(C/C_0)$ versus irradiation time for MO degradation using photocatalysts under different wavelengths (365, 310 and 254 nm) of UV light.

where C_0 and C are the concentrations of model dyes at the irradiation time 0 and t min. Figs. 6 and 7 represent linear plots of $\ln(C/C_0)$ with respective irradiation time for degradation of model dyes such as MO and RhB using the synthesized binary photocatalysts under different wavelengths (i.e. 365, 310 and 254 nm) of UV light irradiation.

Based on the slope of the linear fitted graphs, the calculated k values (Table 2) indicate that the CS-SnO_2 (50:50) nanocomposite has high reaction rate than pure SnO_2 and CS-SnO_2 (75:25). On comparing the degradation rate (under 365 nm irradiation) of the prepared photocatalysts using MO dye, the CS-SnO_2 (50:50) nanocomposite showed 1.77 and 2.74 times higher degradation rate than that of CS-SnO_2 (75:25) nanocomposite and pure SnO_2, respectively. Similarly, in the case of RhB dye, the CS-SnO_2 (50:50) nanocomposite exhibited 1.42 and 1.99 times superior photocatalytic degradation than CS-SnO_2 (75:25) nanocomposite and pure SnO_2, respectively. This is due to the presence of amino and hydroxyl groups as well as high surface area of the synthesized CS-SnO_2 nanocomposite [17,18,23]. On the other hand, increasing the amount of chitosan clearly shows that the crystallinity of the sample has reduced which is in good agreement with the XRD results [24–29]. Thus, comparing with higher CS percentage sample i.e. CS-SnO_2 (75:25), CS-SnO_2 (50:50) nanocomposite exhibits higher degradation of dyes.

Furthermore, recycling process allows finding out the stability and reusability of the materials. Fig. 8 shows the recycling ability of CS-SnO_2 (50:50) nanocomposite. After undergoing recycling process of MO for three times under UV light (365 nm) irradiation, very slight variation was found. Thus, it is concluded that the nanocomposite exhibits good stability and reusability for photocatalytic degradation of dyes under UV light irradiation.

Recently, TiO_2 (P25, 20–30 nm, BET surface area: 50 m^2/g) based chitosan nanocomposite systems were used to degrade various dyes under 6 h of UV light (365 nm) irradiation [14]. Another literature has also reported the photocatalytic degradation of methylene blue solution using ZnO (23 nm) based chitosan nanocomposite under 4 h irradiation of (365 nm) UV light [30–42]. Comparing these reports, the CS-SnO_2 (50:50) nanocomposite system has effectively degraded MO and RhB solution within 100 min of UV light irradiation due to the presence of amino and hydroxyl groups, small size and high surface area. These are confirmed from XRD, TEM and BET analyses.

4. Conclusion

In this work, we successfully prepared novel binary CS-SnO_2 nanocomposites using precipitation method followed by sonication. The photocatalytic degradation results revealed that the prepared binary chitosan-SnO_2 (50:50) nanocomposite was found to have superior photocatalytic degradation efficiency than the pure SnO_2 and chitosan-SnO_2 (75:25) nanocomposite under different wavelengths (365, 310 and 254 nm) of UV light. This is because of the chitosan content in it which has amino and hydroxyl groups that enriched the photocatalytic performance. Maximum photocatalytic activities were found for chitosan-SnO_2 (50:50) nanocomposite under 365 nm irradiation. High photocatalytic degradation efficiency was also due to small size and high surface area of binary chitosan-SnO_2 (50:50) nanocomposite. The stability and reusability of the photocatalyst were also found quite high.

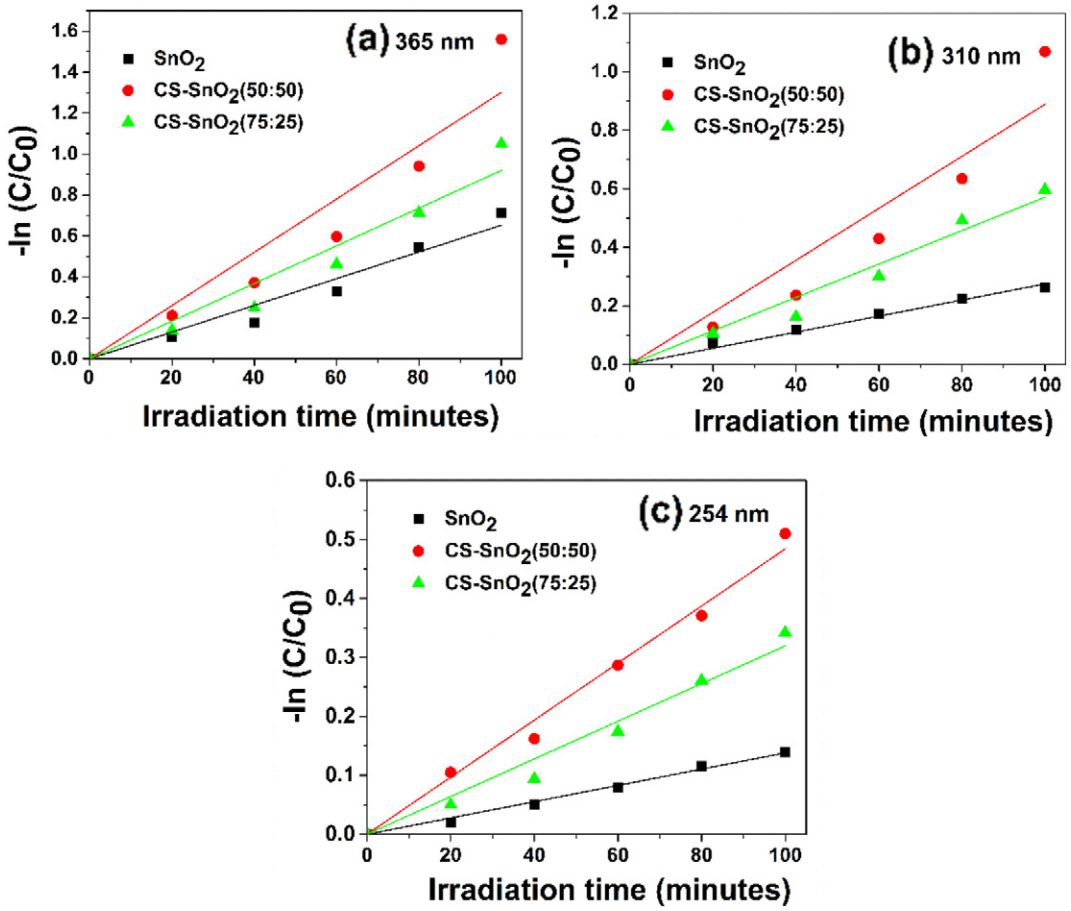

Fig. 7. Plots of $\ln(C/C_0)$ versus irradiation time for RhB dye using photocatalysts under different wavelengths (365, 310 and 254 nm) of UV light.

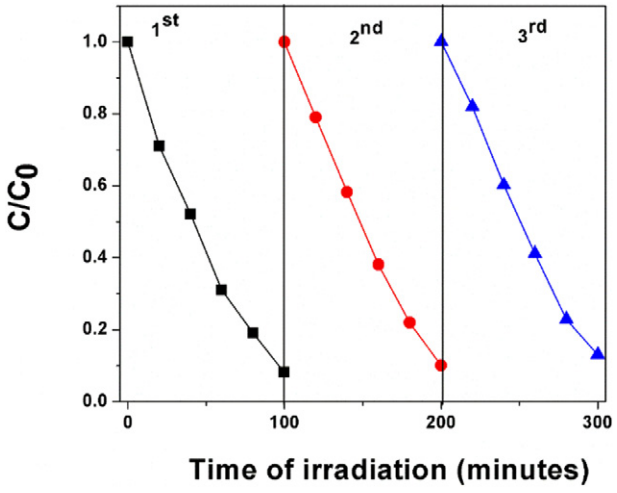

Fig. 8. Recycling ability of CS/SnO_2 (50:50) nanocomposite for degrading MO under 365 nm UV light irradiation.

These results suggest that in future binary chitosan-SnO_2 nanocomposite could be used for environmental remediation.

Acknowledgement

The authors (R.S., F.G.) acknowledge the support of CONICYT through the project FONDECYT No: 3150631 and the postdoctoral fellowship granted to R.S.

References

[1] K. Rajeshwar, M.E. Osugi, W. Chanmanee, C.R. Chenthamarakshan, M.V.B. Zanoni, P. Kajitvichyanukul, R. Krishnan-Ayer, Review heterogeneous photocatalytic treatment of organic dyes in air and aqueous media, J. Photochem. Photobiol. C Photchem. Rev. 9 (2008) 171–192.
[2] Investing in Water and Sanitation: Increasing Access, Reducing Inequalities UN-water Global Analysis and Assessment of Sanitation and Drinking-water GLASS, 2014.
[3] World Water Assessment Programme: Water for People, Water for Life: The UN-world Water Development Report UNESCO-WWAP, 2003.
[4] V.K. Gupta, I. Ali, T.A. Saleh, A. Nayak, S. Agarwal, Chemical treatment technologies for waste-water recycling—an overview, RSC Adv. 2 (2012) 6380–6388.
[5] J. Liqiang, S. Xiaojun, S. Jing, C. Weimin, X. Zili, D. Yaoguo, F. Honggang, Review of surface photovoltage spectra of nano-sized semiconductor and its applications in heterogeneous photocatalysis, Sol. Energy Mater. Sol. Cells 79 (2003) 133–151.
[6] M.M. Khan, S.A. Ansari, D. Pradhan, M.O. Ansari, D.H. Han, J. Lee, M.H. Cho, Band gap engineered TiO_2 nanoparticles for visible light induced photoelectrochemical and photocatalytic studies, J. Mater. Chem. A 2 (2014) 637–644.
[7] S. Kalathil, M.M. Khan, S.A. Ansari, J. Lee, M.H. Cho, Band gap narrowing of titanium dioxide (TiO_2) nanocrystals by electrochemically active biofilms and their visible light activity, Nanoscale 5 (2013) 6323–6326.
[8] R. Saravanan, V.K. Gupta, V. Narayanan, A. Stephen, Comparative study on photocatalytic activity of ZnO prepared by different methods, J. Mol. Liq. 181 (2013) 133–141.
[9] S.A. Ansari, M.M. Khan, M.O. Ansari, J. Lee, M.H. Cho, Highly photoactive SnO_2 nanostructures engineered by electrochemically active biofilm, New J. Chem. 38 (2014) 2462–2469.
[10] M.M. Khan, S.A. Ansari, M.E. Khan, M.O. Ansari, B.K. Min, M.H. Cho, Visible light-induced enhanced photoelectrochemical and photocatalytic studies of gold decorated SnO_2 nanostructures, New J. Chem. 39 (2015) 2758–2766.
[11] A. Nouri, A. Fakhri, Synthesis, characterization and photocatalytic applications of N-, S-, and C-doped SnO_2 nanoparticles under ultraviolet (UV) light illumination, Spectrochim. Acta A Mol. Biomol. Spectrosc. 138 (2015) 563–568.
[12] X. Jia, Y. Liu, X. Wu, Z. Zhang, A low temperature situ precipitation route to designing Zn-doped SnO_2 photocatalyst with enhanced photocatalytic performance, Appl. Surf. Sci. 311 (2014) 609–613.

[13] S.A. Ansari, M.M. Khan, M.O. Ansari, J. Lee, M.H. Cho, Visible light-driven photocatalytic and photoelectrochemical studies of Ag–SnO_2 nanocomposites synthesized using an electrochemically active biofilm, RSC Adv. 4 (2014) 26013–26021.
[14] G. Xiao, H. Su, T. Tan, Synthesis of core–shell bioaffinity chitosan–TiO_2 composite and its environmental applications, J. Hazard. Mater. 283 (2015) 888–896.
[15] N.D. Cuong, T.T. Hoa, D.Q. Khieu, T.D. Lam, N.D. Hoa, N.V. Hieu, Synthesis, characterization, and comparative gas-sensing properties of Fe_2O_3 prepared from Fe_3O_4 and Fe_3O_4-chitosan, J. Alloys Compd. 523 (2012) 120–126.
[16] A. El Shafei, A.A. Okeil, ZnO/carboxymethyl chitosan bionano-composite to impart antibacterial and UV protection for cotton fabric, Carbohydr. Polym. 83 (2011) 920–925.
[17] S.M. Dehaghi, B. Rahmanifar, A.M. Moradi, P.A. Azar, Removal of permethrin pesticide from water by chitosan–zinc oxide nanoparticles composite as an adsorbent, J. Saudi Chem. Soc. 18 (2014) 348–355.
[18] T. Witnoon, T. Permsirivanich, M. Chareonpanich, Chitosan-assisted combustion synthesis of CuO–ZnO nanocomposites: effect of pH and chitosan concentration, Ceram. Int. 39 (2013) 3371–3375.
[19] S.E.S. Saeed, M.M.E. Molla, M.L. Hassan, E. Bakir, M.M.S.A. Mottaleb, M.S.A.A. Mottaleb, Novel chitosan-ZnO based nanocomposites as luminescent tags for cellulosic materials, Carbohydr. Polym. 99 (2014) 817–824.
[20] H. Wang, S. Baek, J. Lee, S. Lim, High photocatalytic activity of silver-loaded ZnO-SnO_2 coupled catalysts, Chem. Eng. J. 146 (2009) 355–361.
[21] G. Rajasudha, H. Shankar, P. Thangadurai, N. Boukos, V. Narayanan, A. Stephen, Preparation and characterization of polyindole–ZnO composite polymer electrolyte with $LiClO_4$, Ionics 16 (2010) 839–848.
[22] L. Zhang, P. Li, Z. Gonga, X. Li, Photocatalytic degradation of polycyclic aromatic hydrocarbons on soil surfaces using TiO_2 under UV light, J. Hazard. Mater. 158 (2008) 478–484.
[23] Y. Sakatani, D. Grosso, L. Nicole, C. Boissie're, Galo J. de A.A. Soler-Illia, C. Sanchez, Optimised photocatalytic activity of grid-like mesoporous TiO_2 films: effect of crystallinity, pore size distribution, and pore accessibility, J. Mater. Chem. 16 (2006) 77–82.
[24] R. Saravanan, et al., ZnO/CdO nanocomposites for textile effluent degradation and electrochemical detection, J. Mol. Liq. 209 (2015) 374–380.
[25] J. Ke, et al., Facile assembly of Bi_2O_3/Bi_2S_3/$MoS2_{n-p}$ heterojunction with layered n-Bi_2O_3 and p-MoS_2 for enhanced photocatalytic water oxidation and pollutant degradation, Appl. Catal. B Environ. 200 (2017) 47–55.
[26] R. Saravanan, E. Sacari, F. Gracia, M.M. Khan, E. Mosquera, V.K. Gupta, Conducting PANI stimulated ZnO system for visible light photocatalytic degradation of colour dyes, J. Mol. Liq. 221 (2016) 1029–1033.
[27] S. Liu, J. Ke, H. Sun, J. Liu, M.O. Tade, S. Wang, Size dependence of uniformed carbon spheres in promoting graphitic carbon nitride toward enhanced photocatalysis, Appl. Catal. B Environ. 204 (2017) 358–364.
[28] S. Rajendran, M.M. Khan, F. Gracia, J. Qin, V.K. Gupta, A. Stephen, Ce^{3+}-ion-induced visible-light photocatalytic degradation and electrochemical activity of ZnO/CeO_2 nanocomposite, Nat.-Sci. Rep. 6 (2016) 31641.
[29] R. Saravanan, et al., ZnO/Ag/Mn_2O_3 nanocomposite for visible light-induced industrial textile effluent degradation, uric acid and ascorbic acid sensing and antimicrobial activities, RSC Adv. 5 (2015) 34645–34651.
[30] S. Dhanavel, E.A.K. Nivethaa, V. Narayanan, A. Stephen, Photocatalytic activity of chitosan/ZnO nanocomposites for degrading methylene blue, Int. J. Chem. Technol. Res. 6 (2014) 1880–1882.
[31] T.A. Saleh, V.K. Gupta, Processing methods and characteristics of porous carbons derived from waste rubber tires: a review, Adv. Colloid Interf. Sci. 211 (2014) 92–100.
[32] V.K. Gupta, R. Kumar, A. Nayak, T.A. Saleh, M.A. Barakat, Adsorptive removal of dyes from aqueous solutions onto carbon nanotubes: a review, Adv. Colloid Interf. Sci. 24–34 (2013).
[33] V.K. Gupta, T.A. Saleh, Sorption of pollutants by porous carbon, carbon nanotubes and fullerene: an overview, Environ. Sci. Pollut. Res. 20 (2013) 2828–2843.
[34] V.K. Gupta, M.R. Ganjali, P. Norouzi, H. Khani, A. Nayak, Shilpi Agarwal, Electrochemical Analysis of some Toxic Metals and Drugs by Ion Selective Electrodes, Crit. Rev. Anal. Chem. 41 (2011) 282–313.
[35] V.K. Gupta, M.R. Ganjali, P. Norouzi, H. Khani, A. Nayak, Shilpi Agarwal, Electrochemical Analysis of some Toxic Metals and Drugs by Ion Selective Electrodes, Crit. Rev. Anal. Chem. 41 (2011) 282–313.
[36] M. Ahmaruzzaman, V.K. Gupta, Rice husk and its ash as low-cost adsorbents in water and wastewater treatment, Ind. Eng. Chem. Res. 50 (2011) 13589–13613.
[37] V.K. Gupta, A. Nayak, S. Agarwal, Bioadsorbents for remediation of heavy metals: current status and their future prospects, Environ. Eng. Res. 20 (1) (2015) 001–018.
[38] Tawfik A. Saleh, Shilpi Agarwal, V.K. Gupta, Synthesis of MWCNT/MnO_2 composites and their application for simultaneous oxidation of arsenite and sorption of arsenate, Appl. Catal. B Environ. 106 (2011) 46–53.
[39] V.K. Gupta, A. Tawfik, Saleh, functionalization of tungsten oxide into MWCNT and its application as a novel catalyst for sun-light-induced degradation of rhodamine B, J. Colloid Interface Sci. 362 (2011) 337–344.
[40] R. Saravanan, S. Karthikeyan, V.K. Gupta, G. Sekaran, V. Narayanan, A. Stephen, Enhanced photocatalytic activity of ZnO/CuO nanocomposites for the degradation of textile dye on visible light illumination, Mater. Sci. Eng. C 33 (2013) 91–98.
[41] V.K. Gupta, A. Mittal, D. Jhare, J. Mittal, Batch and bulk removal of hazardous colouring agent rose bengal by bottom ash, RSC Adv. 2 (2012) 8381–8389.
[42] V.K. Gupta, A. Nayak, S. Agarwal, B. Singhal, Recent advances on potentiometric membrane sensors for pharmaceutical analysis, Combinatorial chemistry & high throughput screening 14 (2011) 284–302.